Pergamon

Phys. Chem. Earth, Vol. 22, No. 1–2, pp. 5–11, 1997

Printed in Great Britain
0079-1946/97 $17.00 + 0.00

PII: S0079-1946(97)00070-0

Modelling Fluid Flow in Rough Fractures: Application to the Hachimantai Geothermal HDR Test Site

P. W. J. Glover and K. Hayashi

Institute of Fluid Sciences, Tohoku University, 2-1-1 Katahira, Aoba-ku, Sendai 980-77, Japan

Received 10 May 1996; accepted 17 December 1996

Abstract. Natural fractures in rocks serve a very important function in the transport of fluid through rocks, as well as in the flow of electrical charge and heat. The first step in understanding these processes must be the complete description and characterisation of the fractures themselves, giving due regard to the often fractal nature of their surfaces. This paper will present a brief analysis of fracture profiles from the Hachimantai geothermal HDR test site in northern Japan, and discuss the implications for fluid flow at this location. The analysis shows that the Hachimantai fracture has a well defined isotropic fractal dimension of 2.305 between the length scales 0.02 mm to 40 mm. The data from the analysis of fracture profiles have been used as input parameters to numerical models of rough fracture surfaces. These surfaces have been used together with a simple fracture closure code to calculate the fluid transmissivity at depth in the Hachimantai fracture. Comparison of the predicted transmissivities produced in this way with those measured by field tests show that the trend and variation of the predicted transmissivities are reproduced well, but are overestimated by a factor representing an overestimation of the fracture aperture of about 1.3.

1 Introduction

There has been an increasing awareness of the great effect fractures have on the mechanical and transport properties of rocks in the last five years. Such fractures may range in scale from extremely small micro-cracks, with a characteristic length scale smaller than the grain size of the rock, up to large fault systems. It is known that many of the statistical geometrical characteristics of natural and hydraulically induced fractures in rocks are fractal. For example the length, aperture, and volume distributions of fractures in crystalline rocks can almost always be described using fractal concepts (e.g. Watanabe and Takahashi, 1995). Additionally, the surface of the fracture has a roughness that is possible to describe in terms of fractal geometry (e.g. Krohn, 1988; Matsuki et al., 1995; Aharonov and Rothman, 1996). It is this last particular geometrical property that we will discuss in this paper.

This paper presents an analysis of profilometry data from the Hachimantai geothermal HDR test site in northern Japan, deriving values for the parameters that describe the fractally rough surfaces found in this rock. This is followed by a discussion concerning how realistic synthetic fractal fractures have been generated using the measured geometrical parameters. Finally there is a description of how these synthetic surfaces have been used in fluid flow and mechanical modelling in order to obtain the transmissivity of the Hachimantai fracture as a function of fluid temperature, fluid pressure and the prevailing confining stress tensor.

2 Analysis of Natural Fractures

The mathematical description of rough surfaces is well reviewed both in books (Peitgen and Saupe, 1988; Russ, 1994) and in many papers (e.g. Brown and Scholz, 1985; Power and Tullis, 1991; Brown, 1995; Matsuki et al., 1995).

Correspondence to: P.W.J. Glover

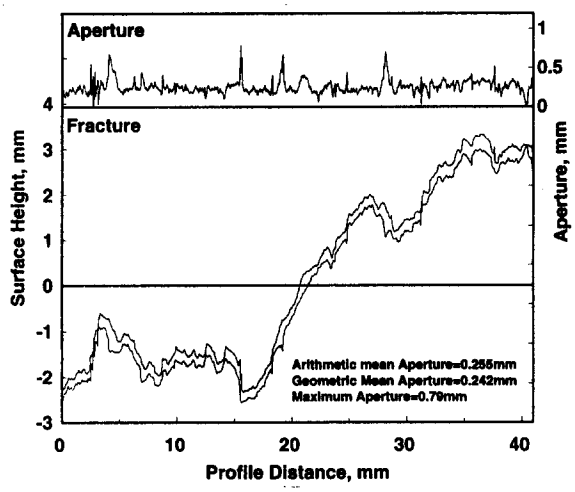

Figure 1. The surface heights for a typical fracture and its associated aperture (Hachimantai fracture; U2D4).

2.1 The Sample Material

The Hachimantai geothermal test field is located in the northern part of the main island of Japan (Honshu) as part of the Γ-project of Tohoku University. It consists of a single hydraulically induced fracture intersected by two boreholes (F1 & EE4). Field pressure tests have examined the hydraulic properties of the borehole and crack system (Hayashi and Abé, 1989). We have used some of these results to compare with the hydraulic properties derived in this work. The core sample containing the original fracture (welded siliceous tuff; borehole EE4 depth 358 m) unfortunately cannot be used for direct profiling because its surface is now significantly damaged. The profiles analyzed in this work were made on a fracture created dynamically in the hydro-fracturing laboratory of the Institute of Fluid Sciences at Tohoku University. The core sample used for this was very closely associated with that containing the original hydrofracture (welded siliceous tuff; borehole EE4 depth 357.5 m).

The sample with its surfaces mated was inserted into a steel V-block jig whose flat faces provide accurate references in such a way that well matched upper and lower surface profiles could be taken. Profiling was carried out with a needle profilometer with a stylus tip of 0.025 mm radius, from a common reference surface. For each fracture surface there were five parallel profiles made in a given direction, each 42 mm long and 10.5 mm apart. The jig was then turned through 90° and five further profiles were made perpendicular to the first set. These profiles were also all 42 mm long and 10.5 mm apart, and arranged so the matrix of profiles on each surface formed a square grid of side 42 mm. The reference jig and use of a reference surface point enabled the profiles from one surface to be aligned accurately with those from the other. The height of each profile was sampled at 4201 equally spaced positions along the profile (x-direction), with a horizontal profile resolution of 0.01 mm. The vertical resolution (z-direction) of this type of profilometer is also 0.01 mm. However, the power spectral density plots indicate that the practical resolution in this application was about 0.009 mm.

2.2 Analytical Procedure

First the profiles were rearranged (inverted and reversed where necessary) to take account of the measurement geometry. The resulting profiles were matched by progressive shearing in the x-direction in order to find the position where the aperture was minimised. The length of the profiles was then reduced to a power of two in order to make the Fourier transformations easier and faster. One profile was then shifted in the z-direction until the two profiles touched at a single point. The aperture at each point in the x-direction was calculated. The minimum (=0), maximum, arithmetic mean, and geometric mean aperture were also calculated. The profiles and apertures have been plotted. Fig. 1 shows a typical example of one of the matched profiles

The DC component and any linear trend was removed from the profiles generated. This was done by regressing a best line to the data and subtracting it from the profile or aperture. A 10% cosine windowing function was applied to the profiles and aperture, and the profiles and aperture were each submitted to a FFT. The output from the FFT for each of the profiles and its related aperture was corrected for windowing, scaled, and normalised to provide power spectral information. The power spectral density (PSD) was plotted as a function of spatial frequency, in double logarithmic space, for each profile and aperture. Regressions were performed on $\log_{10}$ power spectral density data as a function of $\log_{10}$ spatial frequency. The regression information has been used to calculate the fractal dimension of the profiles and apertures, with an associated error. Stacking has been used to calculate the mean power spectral densities for profiles and apertures combining upper and lower surfaces and both profiling directions. These have also been plotted, regressed, fitted in the same way as the individual profiles to produce the analogous mean fractal dimensions and mismatch length scales. Tables 1 and 2 contain only the information for stacked profiles and aper-

Table 1. Properties of profile data from the Hachimantai fracture

Profile Description	Fractal Dimension, D_f and error	Standard Deviation of Asperity Heights, mm
Upper parallel	1.316±0.052	1.549
Upper perpendicular	1.302±0.065	1.033
Lower parallel	1.305±0.042	1.529
Lower perpendicular	1.298±0.045	0.968
All upper profiles	1.310±0.044	1.317
All lower profiles	1.299±0.052	1.280
All profiles	1.305±0.046	1.298

tures due to space constraints. Fig. 2 shows the power spectra of the stacked profiles and apertures. The ratio, $\xi(\lambda)$, of power spectral density for the aperture to that of each of the profiles defining it has also been calculated and plotted. Examples of such a plot can be found in Brown (1995). This type of plot has been used to derive the mismatch length scales, which are also shown in Table 2.

The profiles and aperture created by the removal of the DC trend were also analyzed to produce the probability density and cumulative probability for each. The standard deviation, sample standard deviation, variance and sample variance for each profile and aperture were also calculated. Stacking was used again to obtain the mean statistical data for combinations of profiles for each direction and for each surface (Tables 1 and 2).

2.3 Discussion

In general the fracture profiles show significant long wavelength components, which are missing in their aperture profile. This is reflected in the stacked behaviour (Fig. 2) where the long wavelength flattening of the power spectral density plots for apertures should be compared with the continuing linear increase in the power spectral density plots for profiles. This results from the way that the fracture surfaces are matched at long wavelengths; a geometrical property of fractures in rocks that arises from their formation. In this rock the degree of long wavelength flattening in the aperture is not as well developed as in other rocks. This is due to the presence of missing grains in the surface that induce large local mismatching and result in large local apertures, which are nevertheless at sufficient scale to increase the power of the long wavelength Fourier components.

The fractal dimensions of the profiles are remarkably constant at about 1.30. As expected there is a good correlation between the fractal dimension of the upper and

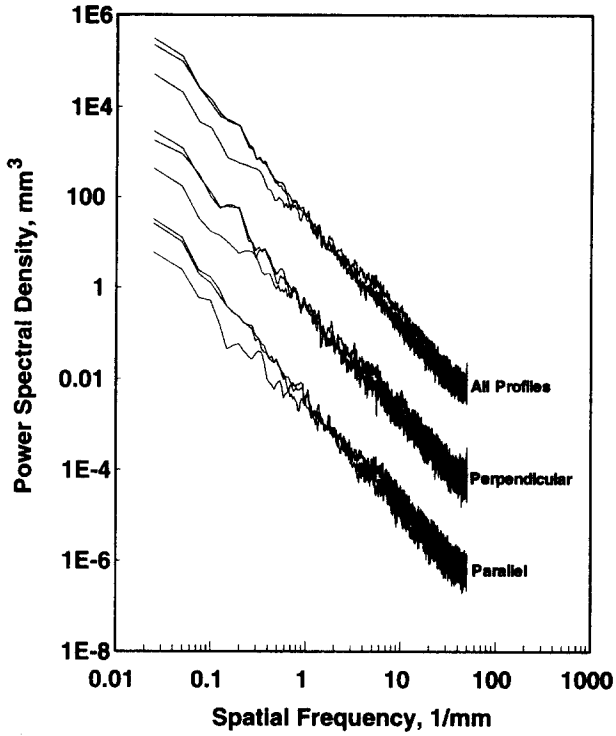

Figure 2. Power spectral density curves for stacked profiles and apertures from the Hachimantai fracture. Each triplet of curves shows the PSD for profiles across the two surfaces, and that of the resulting aperture. All but the lowermost triplet of curves have been progressively shifted by a factor of 100 in the y-direction to avoid overwriting.

lower surfaces of each pair of profiles. There is also no significant difference between the fractal dimension measured for profiles in the two perpendicular directions, indicating the likelihood that the surfaces of the fracture are isotropic at least as far as fractal dimension is concerned. The fractal dimensions of the apertures derived from the matched profiles are always greater than those of the profiles from which they are generated (Tables 1 and 2). There seems to be no significant anisotropy in the fractal dimension of the aperture distribution, as expected.

In all cases the probability functions of the profiles showed a tendency towards Gaussian behaviour. By comparison, the probability density functions of the apertures were better defined by a χ^2-distribution. The standard deviations derived from the probability density functions of surface heights and apertures show more variability than the fractal dimensions from profile to profile and between profiles taken in the two orthogonal directions, but not between the two surfaces (Tables 1 and 2). The standard deviations of surface heights taken parallel to the reference datum are about 50% higher than those in the perpendicular direction for both the upper and lower surfaces. It is expected that this indicates that

Table 2. Properties of Aperture Data from the Hachimantai Fracture

Aperture Code	Fractal Dimension, D_f and error	Mismatch Length Scale, λ_c^1, mm	Mismatch Length Scale, λ_c^2, mm	Mismatch Length Scale, λ_c^a, mm	Mismatch Length Scale, λ_c^b, mm	Mean Aperture, $\langle a_i \rangle_a$, mm	Max. Aperture a_{max}, mm	Standard Deviation of Apertures, mm
Apertures parallel	1.395±0.083	0.85	0.31	1.172	0.294	0.405	2.39	0.370
Apertures perpendicular	1.335±0.044	1.43	0.34	1.147	0.317	0.413	2.20	0.393
All Apertures	1.349±0.066	1.11	0.25	1.172	0.294	0.409	2.39	0.382

either the method used to create the fracture resulted in a mixed mode fracture, or that there is local strength anisotropy within the rock itself. However, the standard deviations of the apertures show no anisotropy, indicating that the anisotropy in surface heights on all profiles are confined to those longer wavelengths at which the fracture is matched, and consequently associated with the mechanism of fracture formation at the scale of the larger grains in the rock.

The four derivations of mismatch length scale shown in Table 2 demonstrate how difficult it is to define a single mismatch length scale for fractures in a particular rock type. The approach used by Brown (1995) is to plot $\xi(\lambda)$ as a function of spatial frequency and to take; (1) the wavelength where the curve crosses the $\xi(\lambda)=1$ line as λ_c^1, and (2) the wavelength where the curve begins to deviate significantly from the $\xi(\lambda)=2$ line as λ_c^2. The first of these length scales, λ_c^1, varies between 0.85 and 1.43 mm, while the second, λ_c^2, varies between 0.25 mm and 0.34 mm. We have defined a further two mismatch length scales , λ_c^a, and λ_c^b. The first, λ_c^a, is that, which when used in creating a synthetic fracture, produces a fracture with a mean aperture equal to that from the profiling measurements. The second, λ_c^b, is that, which when used in creating a synthetic fracture, produces a fracture with an aperture standard deviation equal to that from the profiling measurements. For this fracture λ_c^a and λ_c^b vary between 1.147 mm and 1.172 mm, and between 0.294 mm and 0.317 mm respectively. Of all these definitions of mismatch wavelength it is λ_c^2 and λ_c^b that are closest to the mean grain size of the rock (0.22 mm).

3 Implications for Fluid Flow

If we make the gross assumption that fluid flow at any point i,j in the fracture plane is laminar we can use the Hagen-Poiseuille 'cubic' law that was derived for laminar flow between smooth parallel plates;

$$T_{ij} = \frac{g\, a_{ij}^3}{12\, \nu} \qquad (1)$$

where a_{ij} is the aperture at the position i,j, g is the acceleration due to gravity, and ν is the kinematic viscosity. The stochastic differential equation for constant fluid flow can be solved to give;

$$\langle Q_i \rangle_a = \langle T \rangle_g \langle J_i \rangle_a \qquad (2)$$

where $\langle Q_i \rangle_a$ is the arithmetic mean discharge in the i^{th} direction, $\langle T \rangle_g$ is the geometric mean transmissivity, and $\langle J_i \rangle_a$ is the arithmetic mean hydraulic gradient in the i^{th} direction. The presence of the geometric mean transmissivity is a consequence of the controlling role that small apertures have on the transmissivity.

We have used the aperture measurements described previously to calculate the geometric mean transmissivity by combining Eq. (1) with the definition of the geometric mean of a function, thus;

$$\langle T \rangle_g = \frac{g}{12\, \nu} \left(\exp \left(\frac{\sum_{i,j=1}^{i,j=N} \log_e (a_{ij})}{N^2} \right) \right)^3 \qquad (3)$$

It is difficult to make a valid comparison of a transmissivity calculated this way with data from field experiments because the calculated transmissivities take no account of:

1. The functional dependence of the kinematic viscosity on the fluid temperature and pressure at depth in the reservoir.
2. The effect that the fluid pressure in the reservoir has on the fracture aperture. The fracture aperture at depth may be either smaller or larger than that calculated for one point touching due to the relative sizes of the fluid press-

Table 3. Tuning parameters for synthetic modelling of the Hachimantai fracture

Parameter	Experiment	Model
Isotropic Fractal Dimension of Upper Surface	2.310	2.310
Isotropic Fractal Dimension of Lower Surface	2.299	2.299
Anisotropy of Upper Surface Asperity Heights	1.499	1.499
Anisotropy of Lower Surface Asperity Heights	1.579	1.579
Mismatch Length Scale, λ_c^2, mm	0.250	0.294 λ_c^b
Standard Deviation of Upper Surface Asperity Heights, σ_{upper}, mm	1.317	1.317
Standard Deviation of Lower Surface Asperity Heights, σ_{lower}, mm	1.280	1.280
Standard Deviation of Aperture, σ_{aper}, mm	0.382	0.381
Young's Modulus of Material, GPa	20 (a)	20
Poisson's Ratio of Material	0.13 (b)	0.13

Notes: All experimental data from this work except (a) and (b) which is previously unpublished data from experiments carried out at Tohoku University. The model mismatch length scale λ_c^b is that at which a best match in aperture standard deviation is attained.

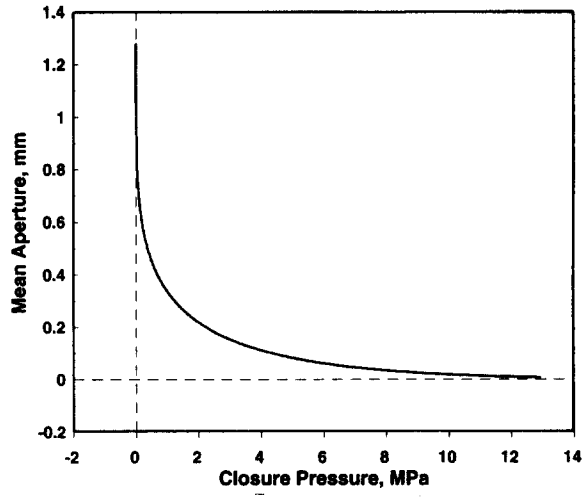

Figure 3. Modelled mean aperture as a function of applied normal stress to synthetic fractures. This curve is the result of 20 applications of the simple closure model described in the text to synthetic fractal apertures created using the geometrical information in Table 3, and differing only in their initial random number seeds.

ure in the reservoir, the values of the principal stresses acting upon the fracture, and the fracture orientation.

We have addressed both of these problems as follows: Inclusion of the pressure and temperature dependence of the fluid kinematic viscosity is relatively trivial. Values of kinematic viscosity as a function of fluid pressure and temperature were taken from a set of steam tables and used in Eq. (3).

Inclusion of the second effect is a non-trivial exercise. We will give a brief account of the procedure here: Synthetic fractal fractures were created to match the parameters measured from the experimental measurements. The parameters used to tune the synthetic fractures to enable them to act as a good statistical model of the real fracture are given in Table 3. The implementation of our code that creates synthetic rough fractures is based upon that of Peitgen and Saupe (1988), with the Brown (1995) modification for implementation of matching between two fracture surfaces below a specified mismatch wavelength. It also includes further modifications that allow the use of surfaces which have anisotropic surface height distributions, and a limited range of probability distributions in addition to the Gaussian one used in this modelling.

Since the Brown (1995) approach to the estimation of mismatch wavelengths from power spectral density ratio curves is open to significant uncertainty, we have opted to chose another method for defining the mismatch wavelength. The mismatch wavelength used in this modelling is that at which the standard deviation of apertures resulting from the synthetic fractures matches that measured in the experimental profiling. We define this mismatch wavelength as λ_c^b. This value tends to differ from λ_c^2 by only a small amount, and is well within the uncertainty in the λ_c^2 measurement. It has the advantage of ensuring that the synthetic has a standard deviation of apertures equal to that of the profiled rock. In our case the value of λ_c^2 was 0.25 mm, and the value of λ_c^b used in the modelling was 0.294 mm (see Tables 2 and 3).

Twenty pairs of such synthetic fractures with the Hachimantai parameters given in Table 3, and differing only in their initial random number seeds, were submitted to a simulated elastic closure (Fig. 3) in the following way. First the fracture surfaces were was translated in the z-direction such that a single location was just touching, and the composite topography of the fracture was calculated. The following (numbered) steps took place within a loop that progressively reduced a datum plane from the maximum of the composite topography (single location touching) to its minimum (contact at all locations) in small increments.

(1) The datum plane level, δ, was reduced by an increment and the new aperture, a_{ij}, was calculated.
(2) The local tangential angles at which asperities contacted were calculated and used to calculate the local values ψ_{ij} of the $<\psi>$ term defined by Brown and Scholz (1985).
(3) The position and number of touching locations were

found.

(4) The local pressure was then calculated at the points where the surfaces touched. These points were defined as those points where the datum plane and the composite topography overlapped. The calculation of pressure assumed that the local pressure is a linear function of the difference between the value of the datum plane and the composite topography, and also used; (a) a locally defined Young's Modulus, E_{ij} (constant in this work and equal to 20 GPa), and (b) the local value of ψ_{ij}.

(5) The overall pressure was then calculated from the local pressures.

(6) Finally the aperture was submitted to a subroutine to calculate its statistical parameters, and these were recorded for each iteration of the loop together with the pressure arrays, touch point arrays, and aperture arrays.

Each iteration of this loop provided the pressure required to reduce the fracture to the current mean aperture, defined by the difference between the composite topography and the datum plane, as well as a map of the number of touching points for each mean aperture. This code assumes linear elastic behaviour with no explicit destruction of asperities, material distribution, and no modification to the local Young's Moduli to represent or result from asperity failure. However the code has been written in such a way that these modifications can be easily added to increase its sophistication. The decision not to incorporate asperity destruction was made on the grounds of simplicity but is supported by experimental work measuring the closure and fluid flow in fractures in Westerly granite (Durham and Bonner, 1994). They observed that surprisingly little asperity destruction occurs especially if the surfaces are well matched. Even if the surfaces are offset and subjected to normal stresses up to 160 MPa, the percentage of the surface subjected to asperity damage remains small (<10%) and confined to local summits.

The closure calculation reported here was carried out independently on each position of the fracture array. The use of synthetic surfaces, that are distributed in three dimensional space and spatially correlated as a result of their fractal nature, makes it unnecessary to include the Hertzian behaviour reported in Greenwood and Williamson (1966), Brown and Scholz (1986), and Matsuki et al. (1996). Goodman (1976) observed empirically that closure of rough fractures follows an exponential law. This has also been observed by Brown and Scholz (1986) and Matsuki et al. (1996) in modelling based on Hertzian contact theory where no explicit account was taken of the spatial correlation

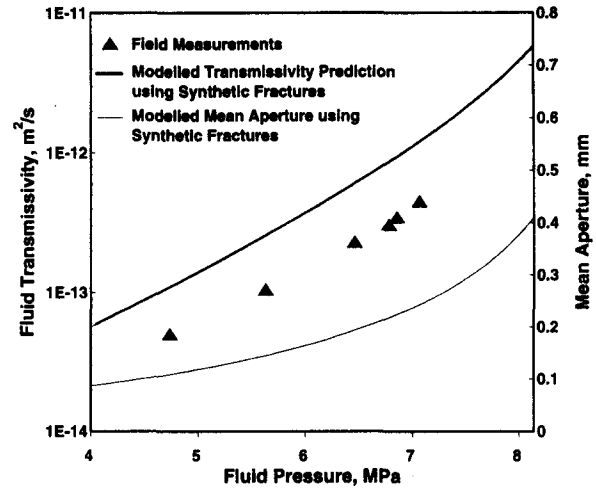

Figure 4. Mean aperture and calculated fluid transmissivity of the Hachimantai fracture at 60 °C as a function of fluid pressure. The aperture is shown as the thin solid line. The thick solid line is the calculated transmissivity Eq. (3). Solid symbols are the results of field measurements of transmissivity after (Hayashi and Abé, 1989).

of the surface. The closure behaviour in Fig. 3 is almost perfectly exponential and shows that even such a simple closure model as the one described above can reproduce the empirically observed behaviour *provided* fractal surfaces are used.

The results from the closure code have been combinedwith the dependence of viscosity upon pore fluid pressure and temperature, and Eq. (3) to provide the transmissivity of the Hachimantai fracture as a function of temperature and pressure. Figure 4 shows the variation of transmissivity as a function of the fluid pressure in the fracture. To create this figure we have assumed that the crack closes and opens elastically with no hysteresis. The maximum fluid pressure in Fig. 4 is that at which the fluid pressure is equal to the normal stress on the fracture at depth in the absence of an applied fluid pressure (8.14 MPa).

Figure 4 also shows the results of 6 experimental determinations of the transmissivity of the fracture from field pressure tests (Hayashi and Abé, 1989). The field data have a trend which matches the transmissivity from the closure of the synthetic surfaces very well, but show that the synthetic transmissivity derived in this way is systematically too high. This is the result of the fracture aperture being overestimated by a factor of about 1.3. It is possible that this is due to several causes. The first is that the assumption in the model that asperities do not break is false. Inclusion of asperity destruction in the closure code

would have the effect of reducing the aperture at a given pressure, and hence also the predicted transmissivity. Such a transmissivity would be closer to that observed experimentally, but it must be realised that in this case the opening of the fracture as fluid pressure increases would be unlikely to follow the same curve as fracture closure, resulting in some hysteresis. Additionally Durham and Bonner (1994) have recently produced experimental evidence that asperity destruction during fracture closure is not as extensive as was once thought. Another cause of the overestimation is that the Hagen-Poiseuille law used to derive the synthetic transmissivity is not valid and that the roughness of the surface exerts some non-laminar influence on the fluid flow. This is likely because it is expected that the majority of the fluid flow in a partially closed fracture exists in channels that are defined by the points where the surfaces touch. Progressive closure increases the tortuosity of these flow paths and may lead to the breakdown of the Hagen-Poiseuille cubic law. Further work clearly needs to be done solving the full Navier-Stokes or Reynolds equations in such fractures. We have made recent advances in modelling fluid flow by solving Reynolds equation in synthetic fractures, and the preliminary results show that the break-down of the cubic law accounts for a large proportion of the overestimation seen in Fig. 4. While recent work by Brown et al. (1995) solving fluid flow with the full Navier-Stokes formulation on simple fracture-like two dimensional models indicates that under closure rock fracture fluid flow estimations using Reynolds equation become unreliable.

4. Conclusions

In recent years there has been considerable progress in both the experimental observation of natural rock fractures, and their theoretical description.

In this work we have measured the geometrical properties of fracture surfaces taken from the Hachimantai geothermal test field located in the northern part of the main island of Japan (Honshu). We observed well developed fractal behaviour on a range of scales from 0.01 mm to the size of the sample (40.96 mm), with an isotropic fractal dimension of fracture surfaces (2.305), and an isotropic fractal dimension of apertures (2.35). Probability density functions for surface height showed a tendency towards Gaussian behaviour with a similar marked anisotropy in both upper and lower profiles. Probability density functions of apertures showed no anisotropy. The estimated mismatch length scales were in the same range as the dominant grain size of the rock (0.22 mm).

These results, together with simple modelling of normal closure and dilatancy, have been used to calculate hydraulic transmissivities which explain the field measurements of transmissivity within the Hachimantai fracture reasonably well, but show a systematic overestimation. Further work needs to be done to ascertain whether this is due to the breakdown of the Hagen-Poiseuille cubic law, or the destruction of surface asperities.

Acknowledgements. The authors would like to thank K. Matsuki, T. Ito and J. Willis-Richards for their help and advice.

References

Aharonov, E. and Rothman, D.H., growth of correlated pore scale structures in sedimentary rocks: A dynamical model, *J. Geophys. Res., 101*, 2973-2987, 1996.

Brown, S.R. and Scholz, C.H., Broad bandwidth study of the topography of natural rock surfaces, *J. Geophys. Res., 90*, 12575-12582, 1985.

Brown, S.R. and Scholz, C.H., Closure of rock joints, *J. Geophys. Res., 91*, 4939-4948, 1986.

Brown, S.R., Simple mathematical model of a rough fracture, *J. Geophys. Res., 100*, 5941-5952, 1995.

Brown, S.R., Stockman, H.W., and Reeves, S.J., Applicability of Reynolds equation for modelling fluid flow between rough surfaces, *Geophys. Res. Lett., 22*, 2537-2540, 1995.

Durham, W.B. and Bonner, B.P., Self-propping and fluid flow in slightly offset joints, *J. Geophys. Res., 99*, 9391-9399, 1994.

Goodman, R.E., *Methods of geological engineering in discontinuous rocks*, 472pp., West Publishing, New York, 1976.

Greenwood, J.A. and Williamson, J., Contact of nominally flat surfaces, *Proc. R. Soc. London, Ser. A, 295*, 300-319, 1966.

Hayashi, K. and Abé, H., Evaluation of hydraulic properties of the artificial subsurface system in Higashihachimantai geothermal model field, *J. Geotherm. Res. Japan, 11 (3)*, 203-215, 1989.

Krohn, C.E., Sandstone fractal and euclidean pore volume distribution, *J. Geophys. Res., 93*, 3286-3296, 1988.

Matsuki, K., Kojima, T., and Murai, T., Surface roughness and initial aperture distribution of a small scale hydraulic fracture in a granite (in Japanese with English abstract and diagrams), *J. Geotherm. Res. Japan, 17 (3)*, 213-232, 1995.

Matsuki, K., Lee, J.J., and Kojima, T., A simulation of the closure of a small scale hydraulic fracture in a granite (in Japanese with English abstract and diagrams), *J. Geotherm. Res. Japan, 18 (1)*, 27-37, 1996.

Peitgen, H-O. and Saupe, D. (Eds.), *The science of fractal images*, Springer-Verlag, New York, 1988.

Power, W.L. and Tullis, T.E., euclidean and fractal models for the description of rock surface roughness, *J. Geophys. Res., 96*, 415-424, 1991.

Russ, J.C., *Fractal surfaces*, 309pp, Plenum, New York, 1994.

Watanabe, K. and Takahashi, H., Fractal geometry characterization of geothermal reservoir networks, *J. Geophys. Res., 100*, 521-528, 1995.